



Intercomparison of IBBCEAS, NitroMAC and FTIR for HONO, NO₂ and HCHO measurements during the reaction of NO₂ with H₂O vapor in the atmospheric simulation chamber of CESAM

Hongming Yi^{1*}, Mathieu Cazaunau², Aline Gratien², Vincent Michoud², Edouard Pangui², Jean-Francois Doussin², Weidong Chen¹

¹Laboratoire de Physicochimie de l'Atmosphère, Université du Littoral Côte d'Opale, 59140 Dunkerque, France

²Laboratoire Interuniversitaire des Systèmes Atmosphériques, CNRS UMR7583, Universités Paris-Est-Créteil et Université de Paris Diderot, 94010 Créteil, France

*now with Department of Civil and Environmental Engineering, Princeton University, Princeton, NJ 08544, USA

10 *Correspondence to:* Jean-Francois Doussin (Jean-Francois.Doussin@lisa.u-pec.fr) and Weidong Chen (chen@univ-littoral.fr)

Abstract. We report on applications of ultraviolet light emitted diode based incoherent broadband cavity enhanced absorption spectroscopy (UV-LED-IBBCEAS) technique for optical monitoring of HONO, NO₂ and CH₂O in a simulation chamber. Performance intercomparison of the UV-LED-IBBCEAS with a wet chemistry-based NitroMAC sensor and a FTIR spectrometer has been carried out on real time simultaneous measurement of HONO, NO₂ and CH₂O concentrations during the reaction of NO₂ with H₂O vapor in the CESAM atmospheric simulation chamber. 1-σ (SNR=1) detection limits of 200 pptv for NO₂, 100 pptv for HONO and 5 ppbv for CH₂O over 120 s were found for the UV-LED-IBBCEAS measurement. On the contrary to many set-ups where cavities are installed outside the simulation chamber, we describe here an original in-situ permanent installation. The intercomparison results demonstrate that IBBCEAS is a very well suitable technique for in situ simultaneous measurements of multiple chemically reactive species with high sensitivity and high precision even if the absorption bands of these species are overlapped. It offers excellent capacity to non-invasive optical monitoring of chemical reaction without any perturbation. For the application to simulation chamber, it has the advantage to provide a spatially integrated measurement across the reactor and hence to avoid point sampling related artefact.

1 Introduction

25 Atmospheric nitrous acid (HONO) is known as a major source of hydroxyl radicals (OH) (Harris et al., 1982; Finlayson-Pitts et al., 2000) in the atmosphere through its photolysis:



which accounts for 30%-60% of the integrated OH source strength (Alicke et al., 2002; Michoud et al., 2012; Griffith et al., 2016). HONO plays hence a crucial role in the atmospheric oxidation capacity that significantly affects the regional air quality and global climate (Finlayson-Pitts et al., 2000; Stutz et al., 2013). Previous studies have shown that known HONO



sources include heterogeneous reactions, homogeneous gas-phase reactions, direct emission, surface photolysis, and biological processes, respectively (Spataro et al., 2014). HONO formation through one mostly possible heterogeneous reaction of NO₂ with water (H₂O) on surfaces is as follows:



35 HONO can be also formed through homogeneous chemistry with the following reaction:



Though it is generally agreed that heterogeneous NO₂ chemistry (reaction R2) is probably among the most important sources of HONO (Finlayson-Pitts et al., 2000; Spataro et al., 2014), modelled HONO concentrations are often significantly below observed values (Vogel et al., 2003; Lammel et al., 1996). The sources of HONO and the mechanisms of HONO formation in the troposphere are still under debate (Kleffmann et al., 2007; Sörgel et al., 2011; Li et al., 2014). Although laboratory studies show that H₂O vapor and surface adsorbed H₂O both play an important role in the conversion process from NO₂ to HONO (Finlayson-Pitts et al., 2000; Spataro et al., 2014), the investigations regarding the influence of H₂O on the NO₂ and HONO chemistry in the real atmosphere remain a highly discussed topics (Stutz et al., 2004; Michoud et al., 2014) and a well-accepted parameterization is still to come. Scientific questions remain about its sources, sinks, and vertical profile in the atmosphere (Young et al., 2012; VandenBoer et al., 2013) that will require high precision measurements. In particular, to disentangle the complex mechanisms that are interplaying and affect HONO atmospheric burden, the scientific community needs reliable high frequency assessment of the concentration change of HONO. In both laboratory studies and atmospheric field campaign, these measurements are challenging due to HONO reactivity and solubility which can cause sampling losses and/or positive artifacts in inlet systems of instruments.

50 Existing detection methods can be categorized as wet chemistry (WC), mass spectrometry (MS) and optical spectroscopy. The wet chemical methods are sensitive. They generally rely on conversion of HONO into nitrite ion (NO₂⁻) following by absorbing dye conversion (Kleffmann et al., 2006) and may be susceptible to chemical interferences and sampling artifacts (Stutz et al., 2010). Moreover, calibrations of the instruments based on WC and MS are difficult, because no permanently stable calibration mixtures exist for HONO.

55 Intercomparison of ambient HONO measurement instruments have been carried out between differential optical absorption spectroscopy (DOAS) and long path absorption photometer (LOPAP) (Kleffmann et al., 2006); between DOAS, mist-chamber/ion chromatograph (MC/IC), stripping coil-visible absorption photometry (SC-AP), ion drift-chemical ionization mass spectrometry (ID-CIMS), and quantum cascade-tunable infrared laser differential absorption spectroscopy (QCL-TILDAS) (Pinto et al., 2014); between LOPAP and NitroMAC (French acronym for "continuous atmospheric measurements of nitrogenous compounds") (Afif et al., 2016); between LOPAP and incoherent broadband cavity enhanced absorption spectroscopy (IBBCEAS) (Wu et al., 2014); between LOPAP, Fourier transform infrared spectrometer (FTIR) and differential photolysis (Reed et al., 2016). Quite frequently, intercomparison between in point and long-path measurements exhibited significant discrepancies with uncertainties of 10%-25% for HONO concentrations from ten-ppbv to ten-ppbv range.



65 Calibration-free, high-sensitivity, direct HONO measurement with UV-IBBCEAS is capable of providing accurate and fast quantitative analysis of HONO concentration variation within its lifetime, which is crucial to improve the understanding of the atmospheric behaviour of HONO.

In the present work, we report on the development of an ultraviolet light emitted diode (UV-LED) based UV-IBBCEAS instrument for simultaneous measurement of wider concentrations at natural conditions of HONO (100 pptv-30 ppbv), NO₂ (100 pptv-120 ppbv) and CH₂O (3-150 ppbv) during the processes of HONO generation through NO₂ reaction with H₂O in a simulation chamber. HONO, NO₂, CH₂O and H₂O vapor concentrations were real time tracking at well controlled conditions. Intercomparison measurements of HONO concentration by UV-IBBCEAS vs. NitroMAC and UV-IBBCEAS vs. FTIR; NO₂ concentration by UV-IBBCEAS vs. chemiluminescence and UV-IBBCEAS vs. FTIR were addressed during 3-day in the atmospheric simulation chamber CESAM. In addition, intercomparison measurements of CH₂O concentration by UV-IBBCEAS vs. FTIR was also simultaneously committed at the last 8 hours of the third day. Agreement of uncertainties <10% were acquired for NO₂, HONO and CH₂O.

2 Experimental details

2.1 Intercompared instruments

2.1.1 LED based UV- IBBCEAS set-up

80 The LED based UV-IBBCEAS setup installed on the simulation chamber, which was used for measurements of NO₂, HONO and CH₂O concentrations in the present work, is shown in Fig. 1. A UV-LED (Nichia, NCSU033AT), emitting ~300 mW optical power in the UV spectral region around 365 nm was used as probing light source. The LED source was mounted on a temperature-controlled heat sink made of copper plate to stabilize the output optical intensity and spectral profile of the LED emission. The temperature of the copper plate was stabilized at 20 °C within ±0.01 °C by means of a single-stage thermoelectric cooler (TEC, PE-063-08-15, Supercool) associated with a temperature sensor (PT100, RTD). A laser diode controller (LDC501, Stanford Research System) was used to supply electric power for both the TEC and the UV-LED. High-finesse optical cavity was formed with two high-reflectivity mirrors (Layertec GmbH) that were installed on the simulation chamber walls facing each other (Fig. 2), separated by the diameter of the cylindrical CESAM chamber, $L=2.13\pm 0.05$ m. The cavity mirrors had 25 mm in diameter and 2 m radius of curvature. The experimentally measured reflectivity of the mirrors is shown in Fig. 3(a) between 350 and 380 nm with a peak value of $R\sim 99.95\%$ at 360 nm. The enhancement factor of the cavity is wavelength-dependent $F=1/(1-R(\lambda))$, ranging from $F=2000$ at $\lambda=365$ nm to $F=1250$ at $\lambda=378$ nm, corresponding to equivalent absorption path lengths through the intra-cavity sample between 4.2 and 2.6 km. Light from the LED was focused with lens L1 (BK7, $f=75$ mm) into the optical cavity. In order to avoid CCD spectrometer saturation at the edges of high reflectivity range of the cavity mirrors, a band-pass filter (Semrock 340-390 nm) was placed between lens L1 and the cavity to block the light at undesirable wavelengths. The diameter (~10 mm) of the light beam injected into the cavity was



controlled with an iris. The light transmitted through the cavity was collected through lens L2 (BK7, $f=75$ mm) to a multimode optical fiber (1000 μm in diameter) and coupled to a CCD spectrometer (QE65000, Ocean optics). The spectrometer allowed covering the whole 190–480 nm spectral range with a spectral resolution of 0.59 nm around 365 nm (this spectral resolution is sufficient for selective recognition of the structured broadband absorption of NO_2 , CH_2O and HONO). The measured spectra from the spectrometer were recorded by a laptop computer through a USB interface.



2.1.2 Wet chemical technique

NitroMAC is an analytical instrument developed for semi-continuous measurement of atmospheric HONO. Based on the original work of (Huang et al., 2002), the concept of NitroMAC relies on a wet chemical derivatization and detection of absorption in the visible at 540 nm using high performance liquid chromatography (HPLC). The instrument has been described in detail in another reference (Afif et al., 2016), but in the present study the instrument was equipped with a dedicated external sampling unit similar to the one of LOPAP instrument (Villena et al., 2011) to minimize potential artefact in the sampling line. Sample from simulation chamber is pumped into NitroMAC with a flow rate of 2 L/min. HONO is hence sampled in a temperature-controlled stripping coil by a fast-chemical reaction in the stripping reagent as soon as a few centimeters (ca. 5 cm) from the chamber port. It is right away converted by dissolution in a buffer phosphate solution and followed by derivatization of nitrite to a highly light-absorbing azo-dye with sulfanilamide (SA) and N-(1-naphthyl)-ethylenediamine (NED) and then transferred to the analytical unit. The operation mode for this instrument consists of two coils connected in series. The arrangement of the two identical coils in series allows the determination of sampling efficiency or the evaluation of possible interferences in HONO measurements. The HONO concentration is calculated by subtracting the signal of the second coil from the signal of the first coil, and finally determined from integration of the peak and a calibration calculation. NaNO_2 standard solutions was used to calibrate NitroMAC. The performance of this instrument in terms of detection limit was found to be around 3 pptv with an optimal integration time of 10 min. The relative standard deviation is 2%, and the relative expanded measurement uncertainty is 12% with signal to noise ratio of 2 (2σ) (Michoud et al., 2014).



2.1.3 FT-IR spectrometer

A Fourier Transform Infra-Red (FTIR) spectrometer equipped with a White type multipass cell was used. Its main purpose was to derive unambiguous NO_2 measurements in order to determine IBBCEAS mirror reflectivity. This spectrometer (model: Bruker® Tensor 37TM) is equipped with a liquid nitrogen cooled MCT detector and a globar source. The multipass cell consists of three high reflectivity gold coated mirrors with a base length of 1.9 m. The configuration of this White cell provided 96 times multiple reflections between three mirrors, thus offered a total effective optical path length of 182 ± 1 m. The multiple path system was crossing the chamber in the same plane as the IBBCEAS pathway with an angle of 60° between the two main optical axis (see Fig. 1–insert). The FTIR system records spectra in the infrared range between 500 and 4000 cm^{-1} with an optimal resolution of 0.5 cm^{-1} . Typical experiment leads to the acquisition of hundreds of FTIR





spectra. To perform the analysis of huge datasets, a home-made software algorithm was written to retrieve NO₂ concentrations. Typical detection limits in absorption spectra recorded by co-adding 100 scans (i.e. with an integration time of 5 min) for various gaseous compounds are listed as follows: NO₂ (5 ppbv), Ozone (5 ppbv), HONO (10 ppb), CH₂O (3 ppbv) or HNO₃ (10 ppbv). 

2.1.4 NO_x analyzer (Chemiluminescence)

In the current experiment, NO₂ is measured using chemiluminescence NO_x (=NO+NO₂) analyzer (Horiba, model APNA360) equipped with molybdenum converter (Sigsby et al., 1973). NO₂ was indirectly measured by first converting it into NO and measuring the sum of NO + NO₂. NO₂ is transformed to NO via a heated, catalyzed converter using molybdenum, and the NO₂ concentration is obtained as the difference between the NO-only measurement and the NO + NO₂ (or NO_x) measurement. Chemiluminescence instruments are typically calibrated with a NO mixture, usually in N₂, which is injected directly or converted to NO₂ via gas-phase titration (Tidona et al., 1988). It is well known that these instruments are subject to strong positive interferences from NO_y (Dunlea et al., 2007) as a large class of nitrogenous compound may be converted on heated Mo converter to produce NO and lead to a chemiluminescence signal on the NO₂ channel. For HONO in particular this interference is considered being quantitative (Villena et al., 2012). In our chemical system, HONO is expected to be the main NO_y interfering with NO₂ measurement, its concentration when available from NitroMAC where subtracted from the APNA 360 “NO₂ channel” to provide “corrected” NO₂ concentration and assuming 100% conversion efficiency for HONO. 

2.1.5 Temperature and humidity sensor

Temperature and relative humidity (RH) inside the simulation chamber were recorded with a temperature and humidity sensor (Vaisala HMP 234). Absolute water vapor concentrations were calculated using the measured RH, the corresponding temperature and the pressure. 

2.2 Intercomparison experiments and set-up

The CESAM simulation chamber is a 4.2 m³ stainless steel chamber. It has been described in detail elsewhere (Wang et al., 2011) and only key information will be recalled here. The CESAM simulation has roughly cylindrical shape of 1.7 m of diameter. When adding the length of the flanges that support the various inlet and instruments (see Fig. 2), it provides a 2 m long diameter that is exploited here to provide the unitary pass length of both the FTIR and IBBCEAS analytical pathway. 

The intercomparison set-up is shown in Fig. 1. The measurement instruments, such as the custom-made UV-LED-IBBCEAS and NitroMAC, a chemiluminescence (CL) NO_x analyzer (HORIBA APNA 370), a FTIR spectrometer (Bruker Tensor 37), are installed around the atmospheric simulation chamber. 

The experiment was performed at room temperature and atmospheric pressure (~23 °C and 760 Torr). Firstly, the chamber was cleaned by pumping down to secondary vacuum (ca. 10⁻⁴ mbar). The chamber was then filled with clean dry air



by mixing 800 mbar of nitrogen produced from the evaporation of a pressurized liquid nitrogen tank (Messer, purity > 99.995 %, H₂O < 5 ppmv) and 200 mbar of oxygen (Air Liquide, ALPHAGAZ™ class 1, purity 99.9 %). The mixture was left ca. 45 minutes for the acquisition of recording instrument background. 500 µl of gaseous NO₂/N₂O₄ mixture was then introduced with a gas-tight syringe (from an NO₂ cylinder: Air Liquide™, Alphagaz™ 99.9% purity) leading to about 120 ppbv of NO₂ in the CESAM chamber. When NO₂ concentration inside the chamber stabilized at 120±5 ppbv, water vapor produced in a small pressurize stainless steel vessel filled with ultrapure water (18.2 Mohm, ELGA Maxima). The relative humidity (RH) inside the chamber was allowed to increase to ~60% at 23 °C (corresponding to an absolute H₂O vapor mixing ratio of ~1.6%).

Under these conditions, as described by Wang et al. (2011), a significant gas-phase HONO is systematically observed. As described in the literature (Finlayson-Pitts et al., 2000; Lammel et al., 1995; Spataro et al., 2014). It is generated through heterogeneous formation on chamber inner surfaces via a complex reaction of NO₂ with adsorbed H₂O chamber walls. All the instruments (UV-IBBCEAS, FTIR, NitroMAC, NO_x analyzer, temperature and humidity sensor, pressure gauge) simultaneously recorded the relevant data (including NO₂, HONO, NO and H₂O concentrations, temperature and pressure) for data analysis and instrument intercomparison. Absolute NO₂ concentrations obtained by FTIR were used for the determination of cavity mirror reflectivity.

Four NO₂ injections in the presence of humid air were organized during the four days of experiments. During the last experiment, an injection of formaldehyde (HCHO) was performed to allow the investigation of the sensitivity of the UV-IBBCEAS data analysis to the interferences in the UV range. Formaldehyde was prepared by sublimating commercial paraformaldehyde (CH₂O)_n (Fluka, “extra pure” grade) under vacuum in a glass line and collected at a known pressure in a bulb of known volume. This quantity was then flushed into the chamber with a gentle flow of pure nitrogen. A controlled dilution flow was allowed to the chamber to induce a forced decrease of the sampled concentrations and hence testing the quantification performance of the various analytical devices across a few orders of magnitudes. This process explains the peak shape formed of a straight injection step followed by an exponential decay of the various experiences.

2.3 Data analysis

2.3.1 UV-LED-IBBCEAS

In an IBBCEAS experiment, the transmitted spectra $I_0(\lambda)$ from the cavity without absorbing species are firstly measured by filling the cavity with pure N₂ or zero air, and then the spectra $I(\lambda)$ in the presence of target sample are recorded. The absorption by molecular species, Rayleigh scattering by gas mixture $\alpha_{\text{Ray}}(\lambda)$, Mie scattering by particles $\alpha_{\text{Mie}}(\lambda)$ and absorption by particle $\alpha_{\text{abs-particle}}(\lambda)$ contribute to optical light extinction in the cavity, the total optical extinction coefficient $\alpha(\lambda)$ can be given as below (Yi et al., 2016):

$$\alpha(\lambda) = \left(\frac{1 - R(\lambda)}{d} + \alpha_{\text{Ray}}(\lambda) + \alpha_{\text{Mie}}(\lambda) + \alpha_{\text{abs-particle}}(\lambda) \right) \times \left(\frac{I_0(\lambda)}{I(\lambda)} - 1 \right) \quad (1)$$



190 where d is the distance between two cavity mirrors. 

In the present work of gas-phase chemical reaction in the simulation chamber filled by zero air, the chamber is free of particles, thus $\alpha_{\text{Mic}}(\lambda) \approx 0$ and $\alpha_{\text{abs-particle}}(\lambda) \approx 0$. The mirror reflectivity can be determined by using a known-concentration NO_2 sample:

$$R(\lambda) = 1 - d \left(\alpha_{\text{NO}_2} \times \frac{I_{\text{NO}_2}(\lambda)}{I_{\text{Zero air}}(\lambda) - I_{\text{NO}_2}(\lambda)} - \alpha_{\text{zero air}}^{\text{Ray}} \right) \quad (2)$$

195 where I_{NO_2} and $I_{\text{zero air}}$ are the transmitted LED light intensities through the cavity containing NO_2 and zero air, respectively, α_{NO_2} is the absorption coefficient of NO_2 and $\alpha_{\text{Ray-zero air}}$ is the Rayleigh scattering coefficient by zero air between 350 nm and 380 nm ($\alpha_{\text{Ray-zero air}} \sim 10^{-8} \text{ cm}^{-1}$). To do so, about 100-200 ppbv NO_2 (absolute NO_2 concentrations were determined by the FTIR spectrometer) was injected in the simulation chamber. Using the known NO_2 concentrations measured in-situ by the FTIR spectrometer and Rayleigh scattering cross section of zero air (see Fig. 3(b)), the mirror reflectivity can be deduced
200 from Eq. (2), as shown in Fig. 3(a). With the measured mirror reflectivity $R(\lambda)$, the real cavity length d , and absorption cross sections $\sigma(\lambda)$ of the target gas from a common database, target gas concentrations can be simultaneously retrieved using a least-squares fit to the experimentally measured absorption coefficient $\alpha(\lambda)$:

$$\alpha(\lambda) = \frac{1 - R(\lambda)}{d} \times \left(\frac{I_0(\lambda)}{I(\lambda)} - 1 \right) = n_{\text{NO}_2} \cdot \sigma_{\text{NO}_2}(\lambda) + n_{\text{HONO}} \cdot \sigma_{\text{HONO}}(\lambda) + n_{\text{CH}_2\text{O}} \cdot \sigma_{\text{CH}_2\text{O}}(\lambda) + a\lambda^2 + b\lambda + c \quad (3)$$

where $\sigma_{\text{NO}_2}(\lambda)$, $\sigma_{\text{HONO}}(\lambda)$ and $\sigma_{\text{CH}_2\text{O}}(\lambda)$ are the reference absorption cross sections (in $[\text{cm}^2/\text{molecule}]$) of NO_2 , HONO and
205 CH_2O species (see Fig. 3(b)), respectively. As shown in Fig. 3(a), the chosen UV-LED emission covers an absorption band of 350-380 nm including NO_2 , HONO, and CH_2O contributions. The reference cross sections of NO_2 (Voigt et al., 2002), HONO (Stutz et al., 2000) and CH_2O (Meller et al., 2000) were convoluted with the instrument function of approximate 0.59 nm (the spectrometer resolution). n_{NO_2} , n_{HONO} and $n_{\text{CH}_2\text{O}}$ are the concentrations (number densities) to determine for NO_2 , HONO and CH_2O , respectively. The second-order polynomial term in Eq. (3) represents the variation in spectral baseline
210 which could arise from gas scattering, LED intensity fluctuations, and other unspecified loss processes. The unknown parameters (number densities n_{NO_2} , n_{HONO} , $n_{\text{CH}_2\text{O}}$, a , b and c) can be extracted using a linear algebraic method known as the singular value decomposition (SVD) method. A Labview based concentration retrieval program was used to simultaneously process the data and provides real-time NO_2 , HONO and CH_2O concentrations. 

Two minutes averaged statistical errors of each individual spectrum was found close to $\sim 1\%$ during data recording with
215 the software procedure which is comparable to the discussion on the IBBCEAS set-up evaluation in several studies (Wu et al., 2012; Gherman et al., 2008; Min et al., 2016). The measurement uncertainty in the retrieval of trace gas mixing ratios are dominated by the uncertainties in the used absorption cross-sections of HONO, NO_2 , and CH_2O ($\pm 5\%$, $\pm 3\%$, and $\pm 3\%$, respectively) (Voigt et al., 2002; Stutz et al., 2000; Meller et al., 2000), in the determination of $(1-R)$ ($\sim 7\%$), in the measurement of I_0/I (0.5%), and in the cavity length determination ($< 1\%$). The total relative uncertainty in the retrieved 



220 concentrations, including statistical uncertainty from the fit and the measurement uncertainty, is approximately estimated to be ~9 % for HONO, ~8% for both NO₂ and CH₂O, respectively.

Typical UV-IBBCEAS spectra (from 351 to 378 nm) of NO₂ (93.3 ppbv, green curve in Fig. 4(a)), HONO (18.0 ppbv, blue curve in Fig. 4(a)) and CH₂O (143.3 ppbv, Fig. 4(b)) as well as the corresponding fits for their concentration retrievals are given in Figs. 4(a,b). Based on the fit residual, the corresponding 1- σ minimum detectable concentration (MDC) for 120 s integration time are 200 pptv for NO₂, 100 pptv for HONO using 355-378 nm region data and 5 ppbv for CH₂O, respectively.

Allan variance analysis was carried out for experimental determination of the stability (corresponding to the optimal integration time) of the UV-IBBCEAS setup. Zero air was used to purge the simulation chamber. Time-series spectra of zero air were recorded with a rate of 1 s per spectrum, about 2000 spectra were acquired for Allan variance study (Wu et al., 2012; Yi et al., 2015). Typical Allan variance curves are plotted in Fig. 5, illustrating a highly desired white noise dominated system stability. As a compromise between detection limit (requiring long integration time) and measurement time response (requiring short measurement time), an integration time of 120 s was selected for use in the present work, which correspond to the measurement precision of 160 pptv for NO₂, 30 pptv for HONO and 3.5 ppbv for CH₂O.

2.3.2 FTIR spectra

235 Infrared spectra were obtained at a resolution of 0.5 cm⁻¹ and derived from the co-addition of approximately 200 scans collected over 5 min. Concentrations of the interested species were determined by subtracting pure reference spectra (brought to the experimental resolution of 0.5 cm⁻¹) from spectra of reaction mixtures using home-made software based on matrix algebra. To guarantee the performance of the automatic routine, selected spectra for each experiment were subtracted manually and results were compared. Spectroscopic information used for the FTIR data analysis are given in table 1. HONO absorption was analyzed from its ν_3 absorption bands around 1263 cm⁻¹ using the synthetic reference spectrum proposed by Barney et al. (Barney et al., 2000) and modified by Barney et al. later (Barney et al., 2001). Mixture FTIR spectra where analyzed using the ANIR deconvolution software (Rodenas et al., 2020) which uses a linear square fitting method to quantitatively analyze experimental spectra through a combination of reference spectra.

3 Results and discussion

245 During the intercomparison experiments in the CESAM atmosphere simulation chamber, time series measurements of NO₂, HONO and CH₂O were simultaneously performed using the UV-LED-IBBCEAS, FTIR spectrometer, NO_x analyzer and NitroMAC.

Before HONO, NO₂ and CH₂O intercomparison measurements, a FTIR was used to measure absolute NO₂ concentrations between 60 and 120 ppbv for determination of the IBBCEAS cavity mirror reflectivity. The measured mirror reflectivity (R) is shown in Fig. 3(a) (red line). During the HONO generation process, NO₂ and H₂O vapor were introduced into the



simulation chamber four times, which correspond to four peaks of NO₂ (as shown in Fig. 7(a)). At the 4th peak in Fig. 7(a), ~160 ppbv CH₂O was also introduced into the chamber to evaluate the UV-LED-IBBCEAS performance for simultaneous detection of NO₂, HONO and CH₂O.

The UV-LED-IBBCEAS spectrometer recorded spectra of the transmitted light intensity with an integration time of 1 s, and 120 such acquisition data were then averaged to produce one datum for $I_0(\lambda)$ or $I(\lambda)$ (i.e. a net acquisition time of 2 min per datum). The response time of the NitroMAC was 10 min for one measurement of HONO concentration. The response time of FTIR for NO₂, HONO, CH₂O and H₂O vapor was 1 min.

3.1 Side-by-side comparison of NO₂ and HONO measurements

Intercomparison of HONO measurements were committed between the UV-LED-IBBCEAS, the NitroMAC and the FTIR, while the measured NO₂ concentrations were compared between the UV-LED-IBBCEAS, the NO_x analyzer and the FTIR.

For in-situ NO₂ monitoring, the correlation between NO_x analyzer and IBBCEAS measurements is not linear. NO_x analyzer over estimated NO₂ concentrations during all measurements, as shown in Fig. 6(a), which was resulted from the well-known positive interferences in the NO_x analyser due to non-selectively converting of all nitrogen containing species inside the chamber into NO (Tidona et al., 1988; Villena et al., 2012) for the indirect measurement of NO₂ concentrations. In the present experiment, the main interferences source was HONO that was transferred into NO in the NO_x analyser, which resulted in an overestimation of the NO₂ concentration. After correction of the HONO contribution to the measured NO₂ concentrations, time series intercomparison measurements of NO₂ between the NO_x analyzer (with HONO correction) and the UV-LED-IBBCEAS are shown in Fig. 6(b), which shows a good agreement between two instruments. Total intercomparison measurements of NO₂ have been then compared between the UV-LED-IBBCEAS, the NO_x analyzer (with HONO correction) and the FTIR, as shown in Fig. 7(a). NO₂ concentrations ranging from 100 pptv to 140 ppbv were investigated during the entire experimental intercomparisons, The corresponding correlation analyses are plotted in Figs. 7(b,c). A linear correlation coefficient of $r^2=98.65\%$ was acquired between interference-corrected NO_x analyzer and IBBCEAS measurements agree well (slope=1.051) with an offset of 0.130 ppbv. The plot of NO₂ measurements by FTIR vs IBBCEAS shown in Fig. 7(c) presents a linear correlation with a $r^2=88.47\%$, the fitted slope and offset are 0.933 and 0.265 ppbv, respectively. This discrepancy of about 7% between FTIR and IBBCEAS mainly comes from the larger relative measurement uncertainty of the FTIR due to its worse detection limit of 10 ppbv compared with that of 200 pptv for IBBCEAS.

Time series intercomparison measurements of HONO by UV-LED-IBBCEAS, NitroMAC and FTIR are shown in Fig. 8(a). To provide a more quantitative intercomparison, a linear regression analysis was performed, weighed with errors of three instruments (IBBCEAS vs. NitroMAC and IBBCEAS vs. FTIR). The comparison of all data and the results of the regression analysis are shown in Figs. 8(b,c). From these results, the HONO concentrations measured by the three instruments display the same variation trend when HONO concentration varied from 0 to 40 ppbv (2nd-4th peaks in Fig. 8(a)).



For the region of 2nd and 3rd peaks in Fig. 8(a), HONO concentrations from NitroMAC are 33% and 35% higher than that from IBBCEAS, respectively. During the 4th HONO generation process (peak 4) in Fig. 8(a), the correlation between the NitroMAC and the IBBCEAS becomes better, NitroMAC measurement is only 8.4% higher than that from IBBCEAS. In this HONO generation process, about 150 ppbv CH₂O was injected into the chamber (Fig. 9(a)). Nevertheless, it is not possible to relate this better correlation result to the presence of formaldehyde. It is hypothesized that the speed of the mixing fan was increased during the last part of the experiment, and by improving the mixing, the point measurement by NitroMAC near by the walls are getting more comparable with the spatially integrated value from the IBBCEAS. The correlation between these two instruments during the entire experiment is $r^2=95.40\%$ (Fig. 8(b)), the gradient of this weighted regression is 1.273 with a y-axis intercept of 0.067 ppbv between the NitroMAC and the IBBCEAS (Fig. 8(b)), showing an overall level of agreement within 27% throughout the entire experiment. Considering the relative measurement uncertainty of 12% for NitroMAC and 9% for IBBCEAS (a total uncertainty of 21% for two-instrument system), **this difference is close from the measurement errors.** A small systematic discrepancy is nevertheless remaining after the uncertainties analysis. It is hypothesized that this disagreement may arise from the sampling volumes of the two techniques and of the HONO generation mechanism. First, IBBCEAS (similarly to FTIR) is providing a spatial average of the concentration across the chamber while NitroMAC is a single point sampler located at the bottom of a side port (see Fig. 1) ca. 20 cm away from the main chamber well-mixed volume. Further, HONO generation is a multiphase process that involves wall and the local wall-to-volume ratio around the NitroMAC inlet is certainly larger than the average wall-to-volume ratio of the CESAM. This may explain why in most of the case NitroMAC values were slightly larger than IBBCEAS. On the other hand, in the IBBCEAS, the final HONO concentrations depend on the selected HONO cross sections (Gratien et al., 2009), the HONO time-concentration profiles in Fig. 8(a) were retrieved using the absorption cross section published by Stutz et al., 2000. If the absorption cross section from another publication (Brust et al., 2000) was used to retrieve HONO concentration, all HONO concentrations in IBBCEAS will increase 23%, which **equal to multiply** a factor of 1.23 **to the** currently presented HONO concentrations in Fig. 8(a). As a result, if HONO concentration retrieval using the absorption cross section from Brust et al. (2000), instead of using the data from Stutz et al. (2000), intercomparison of HONO concentrations between LED-IBBCEAS and NitroMAC will indicate a better agreement (with a linear-fit slope approaching 1).

The correlation and the regression analysis for the comparison between the FTIR and the UV-LED-IBBCEAS (2rd-4th peaks) is given in Fig. 8(c), displaying a slope of 0.952 with a y-axis intercept of 0.250 ppbv and a $r^2=88.91\%$. HONO-concentration variation profile (2rd-4th peaks in Fig. 8(a)) coincides well with each other between IBBCEAS and FTIR. The correlation is **quite excellent (<5%), this 5% discrepancy** is mainly due to the larger measurement uncertainty of HONO by FTIR. FTIR used the integrated HONO absorption band intensity to retrieve HONO concentration, interference from other species is hard to avoid, such as NO₂, HNO₃ and H₂O absorption in the 1200-1300 cm⁻¹ region.



3.2 Interferences and opportunity for formaldehyde measurements using IBBCEAS

315 Formaldehyde is ubiquitous in the atmosphere and is among the most probable interfering species for the deployment of the UV-LED-IBBCEAS as it exhibits strong absorptions between 260 and 360 nm. It is thus important: (a) to investigate any potential artifact during its co-detection with HONO and (b) to evaluate through intercomparison the ability of the newly developed IBBCEAS to reliably quantify it.

During NO₂ and HONO intercomparison campaign around the 4th peak region, about 150 ppbv CH₂O was added into the chamber in order to evaluate potential interference to the IBBCEAS data analysis. The CH₂O concentrations ranging from 0 to 150 ppbv were investigated using UV-LED-IBBCEAS and FTIR, the time series measurements are plotted in Fig. 9(a). A good linear correlation between the measurements by two instruments is obtained with a regression slope of 1.053 and an intercept of 3.653 ppbv ($r^2=97.09\%$), as shown in Fig. 9(b). This measurement intercomparison confirmed the good performance of the measurement of CH₂O using IBBCEAS. This relatively large intercept of 3.653 ppbv is due to the relative low detection limit of 5 ppbv because the used UV-LED emission intensity was very weak at its side wing near 350 nm at which CH₂O was probed (Fig. 2) which degraded significantly the SNR (signal to noise ratio) in the IBBCEAS spectrum of CH₂O. Moreover, the corresponding CH₂O absorption cross section near 350 nm is not the highest for its sensitive measurement. The MDC can be further improved by using a suitable light source with main emission centered between 315-350 nm allowing to probe the strongest CH₂O absorption lines which may lead to a MDC of 0.38 ppbv (Washenfelder et al., 2016; Liu et al., 2020). The present work, with excellent measurements correlation on NO₂, HONO and CH₂O between IBBCEAS and other well-established instruments, shows that the IBBCEAS technique offers the ability of self-calibration for simultaneously measuring concentrations of these three species with high precision without significant interference influence even if their absorption cross sections are overlapped.

4 Conclusion

335 Intercomparison measurements of HONO, NO₂ and CH₂O between IBBCEAS, NitroMAC and FTIR have been performed during the reaction of NO₂ with H₂O vapor in the CESAM atmosphere simulation chamber. The performance of IBBCEAS was evaluated through side-by-side comparison with NitroMAC and FTIR for HONO, with FTIR and NO_x analyzer for NO₂, and with FTIR for CH₂O. The intercomparison of all instruments were found to be in good agreement on the temporal trends and variability in HONO, NO₂ and CH₂O. Exception of measurements near instrument detection limits, no evidence was found for any systematic bias in any of the instruments. Good correlation of better than 93% for NO₂ measurement was obtained among IBBCEAS, NO_x analyzer and FTIR under a well-controlled condition in simulation chamber. Positive interference to the NO₂ concentration measurement using NO_x analyzer was corrected by deduction of HONO contribution.



More than 95% correlation for CH₂O measurement was also acquired between IBBCEAS and FTIR. The measured time-series HONO profiles displayed a relatively large divergence (up to 30%) in absolute concentrations from the
345 intercomparison between IBBCEAS and NitroMAC. NitroMAC indicated somewhat higher HONO concentration than those from the IBBCEAS and the FTIR. This discrepancy ~27% can only be partly attributed to the uncertainty cross sections used for HONO concentration retrieval. A significant fraction of the discrepancy can most probably attribute to the fact that NitroMAC was sampling in point relatively protected from the mixing fan effects and close from the wall i.e. where HONO is being produced. This drawback of our experimental strategy did not harm too seriously our assessment of the IBBCEAS
350 set-up and retrieval thanks to the use of in-situ FTIR, which had the advantage to illustrate well how important it is to perform measurements spatially relevant of the sounded volume. It illustrates well how in-situ spatially averaged measurements are the strategy of choice for the monitoring of reactive species in simulation chambers.

The experimental results and relevant analysis indicated that UV-LED-IBBCEAS owns the advantage of studying chemical dynamics by means of in situ and fast concentration tracking with high-precision without interference influence, it
355 also has the capacity of simultaneously and directly measuring NO₂, HONO and CH₂O in chamber without any sampling by pump and hence without any influence on the chemical reaction on going, which offers its unique advantage of non-invasive monitoring of chemical reaction in chamber. Its absorption line intensity based self-calibration capacity exhibits another advantage compared to the need of complicated calibration process using chemical solutions for wet chemistry based analytical instrument.

360

365



Data availability

The data used in this study are available from the corresponding author upon request (Jean-Francois Doussin (Jean-
370 Francois.Doussin@lisa.u-pec.fr) and Weidong Chen (chen@univ-littoral.fr)).

Author contributions

The manuscript was written through contributions of all authors. All authors have given approval to the final version of the
manuscript.

375

Competing interests

The authors declare that they have no conflict of interest.

Acknowledgments

380 The authors acknowledge financial supports from the French Agence Nationale de la Recherche (ANR) under the CaPPA
(ANR-10-LABX-005) contract, as well as the support in the framework of the CPER CLIMIBIO program funded by Nord-
Pas de Calais Region and the Ministère de l'Enseignement Supérieur et de la Recherche. CNRS-INSU is gratefully
acknowledged for supporting the CESAM chamber as a national facility (<http://cesam.cnrs.fr>). European Union's Horizon
2020 research and innovation program through the EUROCHAMP-2020 Infrastructure Activity under grant agreement
385 n°730997 is also gratefully acknowledged for distributing freely the ANIR deconvolution software as well as Mila Rodenas
and the Centro de Estudios Ambientales del Mediterráneo (CEAM - Valencia) for sharing the software and providing the
guidance in using it.

References

- Affif, C., Jambert, C., Michoud, V., Colomb, A., Eyglunent, G., Borbon, A., Daële, V., Doussin, J.-F. and Perros, P.:
390 NitroMAC: An instrument for the measurement of HONO and intercomparison with a long-path absorption photometer, *J.*
Environ. Sci. (China), 40, 105-113, doi:10.1016/j.jes.2015.10.024, 2016.
- Alicke, B., Platt, U., and Stutz, J.: Impact of nitrous acid photolysis on the total hydroxyl radical budget during the
Limitation of Oxidant Production / Pianura Padana Produzione di Ozono study in Milan, *J. Geophys. Res.*, 107(D22), 8196,
doi:10.1029/2000JD000075, 2002.
- 395 Barney, W. S., Wingen, L. M., Lakin, M. J., Brauers, T., Stutz, J., Finlayson-Pitts, B. J., Infrared absorption cross-section
measurements for nitrous acid (HONO) at room temperature, *J. Phys. Chem. A*, 104(8), 1692-1699, doi:10.1021/jp9930503,
2000.



- Barney, W. S., Wingen, L.M., Lakin, M.J., Brauers, T., Stutz, J., Finlayson-Pitts, B.J., Infrared absorption cross-section measurements for nitrous acid (HONO) at room temperature, *J. Phys. Chem. A*, 105 (16), 4166-4166, 400 doi:10.1021/jp010734d, 2001.
- Bongartz, A., Kames, J., Schurath, U., George, C., Mirabel, P., Ponche, J. L. Experimental determination of HONO mass accommodation coefficients using two different techniques, *J. Atmos. Chem.*, 18, 149–69, doi: 10.1007/BF00696812, 1994.
- Brust, A. S., Becker, K. H., Kleffmann, J., Wiesen, P.: UV absorption cross sections of nitrous acid. *Atmos Environ.*, 34, 13–19, doi:10.1016/S1352-2310(99)00322-2, 2000.
- 405 Dunlea, E. J., Herndon, S. C., Nelson, D. D., Volkamer, R. M., San Martini, F., Sheehy, P. M., Zahniser, M. S., Shorter, J. H., Wormhoudt, J. C., Lamb, B. K., Allwine, E. J., Gaffney, J. S., Marley, N. A., Grutter, M., Marquez, C., Blanco, S., Cardenas, B., Retama, A., Ramos Villegas, C. R., Kolb, C. E., Molina, L. T., and Molina, M. J.: Evaluation of nitrogen dioxide chemiluminescence monitors in a polluted urban environment, *Atmos. Chem. Phys.*, 7, 2691–2704, doi:10.5194/ACP-7-2691-2007, 2007.
- 410 Finlayson-Pitts, B. J. and Pitts, Jr. J. N.: *The chemistry of the Lower and Upper Atmosphere : Theory, experiments and applications*, Academic Press, New-York, NJ, USA, doi:10.1016/B978-0-12-257060-5.X5000-X, 2000.
- Gherman, T., Venables, D. S., Vaughan, S., Orphal, J., and Ruth, A. A.: Incoherent broadband cavity-enhanced absorption spectroscopy in the near-ultraviolet: Application to HONO and NO₂, *Environ. Sci. Technol.*, 42(3), 890-895, doi:10.1021/es0716913, 2008.
- 415 Gratien, A., Lefort, M., Picquet-Varrault, B., Orphal, J., Doussin, J. F., Flaud, J. M.: Experimental intercomparison of the absorption cross-sections of nitrous acid (HONO) in the ultraviolet and mid-infrared spectral regions, *J. Quant. Spectrosc. Radiat. Transf.*, 110(4-5), 256–263, doi:10.1016/j.jqsrt.2008.11.003, 2009.
- Griffith S. M., Hansen, R. F., Dusanter, S., Michoud, V., Gilman, J. B., Kuster, W. C., Veres, P., Graus, M., Warneke, C., Gouw, J. A. de, Young, C., Washenfelder, R., Brown, S. S., Volkamer, R., Stutz, J. S., Flynn, J. H., Grossberg, N., Lefter, B.,
- 420 Alvarez, S. L., Rappenglueck, B., Mielke, L. H., Osthoff, H. D., and Steven, P. S.: Measurements of hydroxyl and hydroperoxy radicals during CalNex-LA: Model comparisons and radical budgets, *J. Geophys. Res. Atmos.*, 121, 4211–4232, doi:10.1002/2015JD024358, 2016.
- Harris, G. W., Carter, W. P. L., Winer, A. M., Pitts, A. M. J., Platt, U., and Perner, D.: Observations of nitrous acid in the Los Angeles atmospheres and implication for prediction of ozone-precursor relationship, *Environ. Sci. Technol.*, 16, 414-425 doi:10.1021/es00101a009, 1982.
- Huang, G., Zhou, X., Deng, G., Qiao, H., and Civerolo, K.: Measurements of atmospheric nitrous acid and nitric acid. *Atmos. Environ.* 36 (13), 2225–2235, doi:10.1016/S1352-2310(02)00170-X, 2002.
- Kagann, R. H., Maki, A. G. Infrared absorption intensities of nitrous acid (HONO) fundamental bands. *J. Quant. Spectrosc. Radiat. Transf.*, 30, 37–44, doi:10.1016/0022-4073(83)90071-7, 1983.
- 430 Kleffmann, J.: Daytime sources of nitrous acid (HONO) in the atmospheric boundary layer, *Chem. Phys. Chem.*, 8, 1137–1144, doi:10.1002/cphc.200700016, 2007.



- Kleffmann, J., Lörzer, J. C., Wiesen, P., Kern, C., Trick, S., Volkamer, R., Rodenas, M. and Wirtz, K.: Intercomparison of the DOAS and LOPAP techniques for the detection of nitrous acid (HONO), *Atmos. Environ.*, 40(20), 3640–3652, doi:10.1016/j.atmosenv.2006.03.027, 2006.
- 435 Lammel, G., and Cape, J. N.: Nitrous acid and nitrite in the atmosphere, *Chem. Soc. Rev.*, 25, 361-369, doi:10.1039/CS9962500361, 1996.
- Li, X., Rohrer, F., Hofzumahaus, A., Brauers, T., Häsel, R., Bohn, B., Broch, S., Fuchs, H., Gomm, S., Holland, F., Jäger, J., Kaiser, J., Keutsch, F. N., Lohse, I., Lu, K., Tillmann, R., Wegener, R., Wolfe, G. M., Mentel, T. F., Kiendler-Scharr, A., and Wahner, A.: Missing Gas-Phase Source of HONO Inferred from Zeppelin Measurements in the Troposphere, *Science*, 440 344, 292-296, doi:10.1126/science.1248999, 2014.
- Liu, J., Li, X., Yang, Y., Wang, H., Kuang, C., Zhu, Y., Chen, M., Hu, J., Zeng, L., Zhang, Y.: Sensitive Detection of Ambient Formaldehyde by Incoherent Broadband Cavity Enhanced Absorption Spectroscopy, *Anal. Chem.*, 92, 2697–2705, doi:10.1021/acs.analchem.9b04821, 2020.
- Meller, R., and Moortgat, G. K.: Temperature dependence of the absorption cross sections of formaldehyde between 223 and 445 323 K in the wavelength range 225-375 nm, *J. Geophys. Res. D*, 105, 7089-7101, doi:10.1029/1999JD901074, 2000.
- Michoud, V., Kukui, A., Camredon, M., Colomb, A., Borbon, A., Miet, K., Aumont, B., Beekmann, M., Durand-Jolibois, R., Perrier, S., Zapf, P., Siour, G., Ait-Helal, W., Locoge, N., Sauvage, S., Afif, C., Gros, V., Furger, M., Ancellet G., and Doussin, J. F.: Radical budget analysis in a suburban European site during the MEGAPOLI summer field campaign, *Atmos. Chem. Phys.* 12(24), 11951-11974, doi:10.5194/acp-12-11951-2012, 2012.
- 450 Michoud, V., Colomb, A., Borbon, A., Miet, K., Beekmann, M., Camredon, M., Aumont, B., Perrier, S., Zapf, P., Siour, G., Ait-Helal, W., Afif, C., Kukui, A., Furger, M., Dupont, J. C., Haeffelin, M., and Doussin, J. F.: Study of the unknown HONO daytime source at a European suburban site during the MEGAPOLI summer and winter field campaigns, *Atmos. Chem. Phys.* 14(6), 2805-2822, doi:10.5194/acp-14-2805-2014, 2014.
- Min, K.-E., Washenfelder, R. A., Dubé, W. P., Langford, A. O., Edwards, P. M., Zarzana, K. J., Stutz, J., Lu, K., Rohrer, F., 455 Zhang, Y., and Brown, S. S.: A broadband cavity enhanced absorption spectrometer for aircraft measurements of glyoxal, methylglyoxal, nitrous acid, nitrogen dioxide, and water vapor, *Atmos. Meas. Tech.*, 9, 423-440, doi:10.5194/amt-9-423-2016, 2016.
- Pinto, J. P., Dibb, J., Lee, B. H., Rappenglück, B., Wood, E. C., Levy, M., Zhang, R.-Y., Lefter, B., Ren, X.-R., Stutz, J., Tsai, C., Ackermann, L., Golovko, J., Herndon, S. C., Oakes, M., Meng, Q.-Y., Munger, J. W., Zahniser, M. and Zheng, J.: 460 Intercomparison of Field Measurements of HONO during SHARP, *J. Geophys. Res. Atmos.*, 119, 5583–5601, doi:10.1002/2013JD020287, 2014.
- Reed, C., Brumby, C. A., Crilley, L. R., Kramer, L. J., Bloss, W. J., Seakins, P. W., Lee, J. D., and Carpenter, L. J.: HONO measurement by differential photolysis, *Atmos. Meas. Tech.*, 9, 2483-2495, doi:10.5194/amt-2016-17, 2016.
- Ródenas, M., Picquet-Varrault, B., and Muñoz, A.: ANIR, a tool for analysis of Infrared spectra, EGU General Assembly 465 2020, Online, 4–8 May 2020, EGU2020-17199, <https://doi.org/10.5194/egusphere-egu2020-17199>, 2020.



- Sigsby, J. E., Black, F. M., Bellar, T. A., and Klosterman, D. L.: Chemiluminescent method for analysis of nitrogen containing compounds in mobile source emissions (NO, NO₂ and NH₃), *Environ. Sci. Technol.*, 7, 51–54, doi:10.1021/es60073a001, 1973.
- Sörgel, M., Regelin, E., Bozem, H., Diesch, J. -M., Drewnick, F., Fischer, H., Harde, H., Held, A., Hosaynali-Beygi, Z.,
470 Martinez, M. and Zetzsch, C.: Quantification of the unknown HONO daytime source and its relation to NO₂, *Atmos. Chem. Phys.*, 11, 10433–10447, doi:10.5194/acp-11-10433-2011, 2011.
- Spataro, F., and Ianniello, A.: Sources of atmospheric nitrous acid: State of the science, current research needs, and future prospects, *J. Air Waste Manage. Assoc.*, 64(11), 1232–1250, doi:10.1016/j.atmosenv.2012.02.041, 2014.
- Stutz, J., Wong, K.W., and Tsai, C.: Field Observation of Daytime HONO Chemistry and its Impact on the OH Radical
475 Budget, in *Disposal of Dangerous Chemicals in Urban Areas and Mega Cities*, I. Barnes and K.J. Rudzinski, Eds., NATO Science for Peace and Security Series C: Environmental Security, Springer, Dordrecht, doi:10.1007/978-94-007-5034-0_1, 2013.
- Stutz, J., Alicke, B., Ackermann, R., Geyer, A., Wang, S., White, A. B., Williams, E. J., Spicer, C.W. and Fast, J. D.: Relative humidity dependence of HONO chemistry in urban areas, *J. Geophys. Res.*, 109, D03307,
480 doi:10.1029/2003JD004135, 2004.
- Stutz, J., Oh, H. J., Whitlow, S. I., Anderson, C., Dibbb, J. E., Flynn, J. H., Rappengluck, B., and Lefer, B.: Simultaneous DOAS and mist-chamber IC measurements of HONO in Houston, TX, *Atmos. Environ.*, 44, 4090–4098, doi:10.1016/j.atmosenv.2009.02.003, 2010.
- Stutz, J., Kim, E. S., Platt, U., Bruno, P., Perrino, C., and Febo, A.: UV-visible absorption cross sections of nitrous acid, *J. Geophys. Res.*, 105, 14585–14592, doi:10.1029/2000JD900003, 2000.
- Svensson, R., Ljungstrom, E., and Lindqvist, O.: Kinetics of the Reaction between Nitrogen-Dioxide and Water-Vapor, *Atmos. Environ.*, 21, 1529–1539, doi:10.1016/0004-6981(87)90315-5, 1987.
- Tidona, R. J., Nizami A. A., and Cernansky, N. P.: Reducing Interference Effects in the Chemiluminescent Measurement of Nitric Oxides from Combustion Systems, *JAPCA* 38(6), 806–811, doi:10.1080/08940630.1988.10466421, 1988.
- 490 VandenBoer, T. C., Brown, S. S., Murphy, J. G., Keene, W. C., Young, C. J., Pszenny, A. A. P., Kim, S., Warneke, C., de Gouw, J. A., Maben, J. R., Wagner, N. L., Riedel, T. P., Thornton, J. A., Wolfe, D. E., Dube, W. P., Ozturk, F., Brock, C. A., Grossberg, N., Lefer, B., Lerner, B., Middlebrook, A. M., and Roberts, J. M.: Understanding the role of the ground surface in HONO vertical structure: High resolution vertical profiles during NACHTT-11, *J. Geophys. Res.*, 118, 10155–10171, doi:10.1002/jgrd.50721, 2013.
- 495 Villena, G., Bejan, I., Kurtenbach, R., Wiesen, P., and Kleffmann, J.: Development of a new Long Path Absorption Photometer (LOPAP) instrument for the sensitive detection of NO₂ in the atmosphere, *Atmos. Meas. Tech.*, 4, 1663–1676, doi:10.5194/amt-4-1663-2011, 2011.
- Villena, G., Bejan, I., Kurtenbach, R., Wiesen, P., and Kleffmann, J.: Interferences of commercial NO₂ instruments in the urban atmosphere and in a smog chamber, *Atmos. Meas. Tech.*, 5, 149–159, doi:10.5194/amt-5-149-2012, 2012.



- 500 Vogel, B., Vogel, H., Kleffmann, J., Kurtenbach, R.: Measured and simulated vertical profiles of nitrous acid-Part II. Model simulations and indications for a photolytic source, *Atmos. Environ.*, *37*, 2957–2966, doi:10.1016/S1352-2310(03)00243-7, 2003.
- Voigt, S., Orphal, J., Burrows, J. P.: The temperature and pressure dependence of the absorption cross-sections of NO₂ in the 250–800 nm region measured by Fourier-transform spectroscopy, *J. Photochem. Photobiol. A: Chem.*, *149*, 1–7, doi:10.1016/S1010-6030(01)00650-5, 2002.
- 505 Wang, J., Doussin, J. F., Perrier, S., Perraudin, E., Katrib, Y., Pangu, E., and Picquet-Varrault, B.: Design of a new multi-phase experimental simulation chamber for atmospheric photochemistry, aerosol and cloud chemistry research, *Atmos. Meas. Tech.*, *4*, 2465–2494, doi:10.5194/amt-4-2465-2011, 2011.
- Washenfelder, R. A., Attwood, A. R., Flores, J. M., Zarzana, K. J., Rudich, Y., and Brown, S. S.: Broadband cavity-enhanced absorption spectroscopy in the ultraviolet spectral region for measurements of nitrogen dioxide and formaldehyde, *Atmos. Meas. Tech.*, *9*, 41–52, doi:10.5194/amt-9-41-2016, 2016.
- 510 Wu, T., Zha, Q., Chen, W., Xu, Z., Wang, T., and He, X.: Development and deployment of a cavity enhanced UV-LED spectrometer for measurements of atmospheric HONO and NO₂ in Hong Kong, *Atmos. Environ.*, *95*, 544–551, doi:10.1016/j.atmosenv.2014.07.016, 2014.
- 515 Wu, T., Chen, W., Fertein, E., Cazier, F., Dewaele, D., and Gao, X.: Development of an open-path incoherent broadband cavity-enhanced spectroscopy based instrument for simultaneous measurement of HONO and NO₂ in ambient air, *Appl. Phys. B*, *106*, 501–509, doi:10.1007/s00340-011-4818-3, 2012.
- Xu, Z., and Lin, M., Kinetics and mechanism for the CH₂O + NO₂ reaction: A computational study. *Int. J. Chem. Kinet.*, *35*: 184–190, doi:10.1002/kin.10115, 2003.
- 520 Yi, H., Wu, T., Wang, G., Zhao, W., Fertein, E., Coeur, C., Gao, X., Zhang, W., and Chen, W.: Sensing atmospheric reactive species using light emitting diode by incoherent broadband cavity enhanced absorption spectroscopy, *Opt. Express*, *24*, A781–A790, doi:10.1364/OE.24.00A781, 2016.
- Yi, H., Maamary, R., Gao, X., Sigrist, M. W., Fertein, E., Chen, W.: Short-lived species detection of nitrous acid by external-cavity quantum cascade laser based quartz-enhanced photoacoustic absorption spectroscopy, *Appl. Phys. Lett.*, *106*, 101109, doi:10.1063/1.4914896, 2015.
- 525 Young, C. J., Washenfelder, R. A., Roberts, J. M., Mielke, L. H., Osthoff, H. D., Tsai, C., Pikel'naya, O., Stutz, J., Veres, P. R., Cochran, A. K., VandenBoer, T. C., Flynn, J., Grossberg, N., Haman, C. L., Lefter, B., Stark, H., Graus, M., de Gouw, J., Gilman, J. B., Kuster, W. C., and Brown, S. S.: Vertically resolved measurements of nighttime radical reservoirs in Los Angeles and their contribution to the urban radical budget, *Environ. Sci. Technol.*, *46*, 10965–10973, doi:10.1021/es302206a, 2012.
- 530

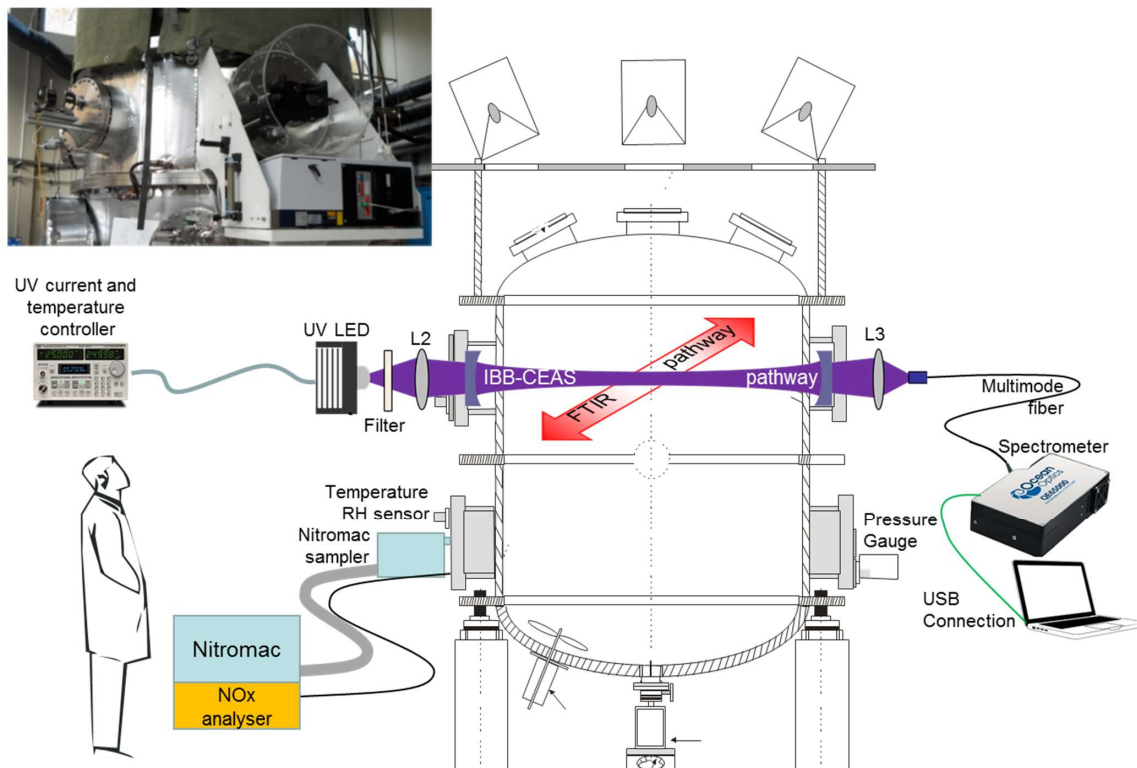


535

Table 1 Absorption bands adopted by FTIR for NO₂, HONO, CH₂O and H₂O measurement. IBI: Integrated Band Intensities

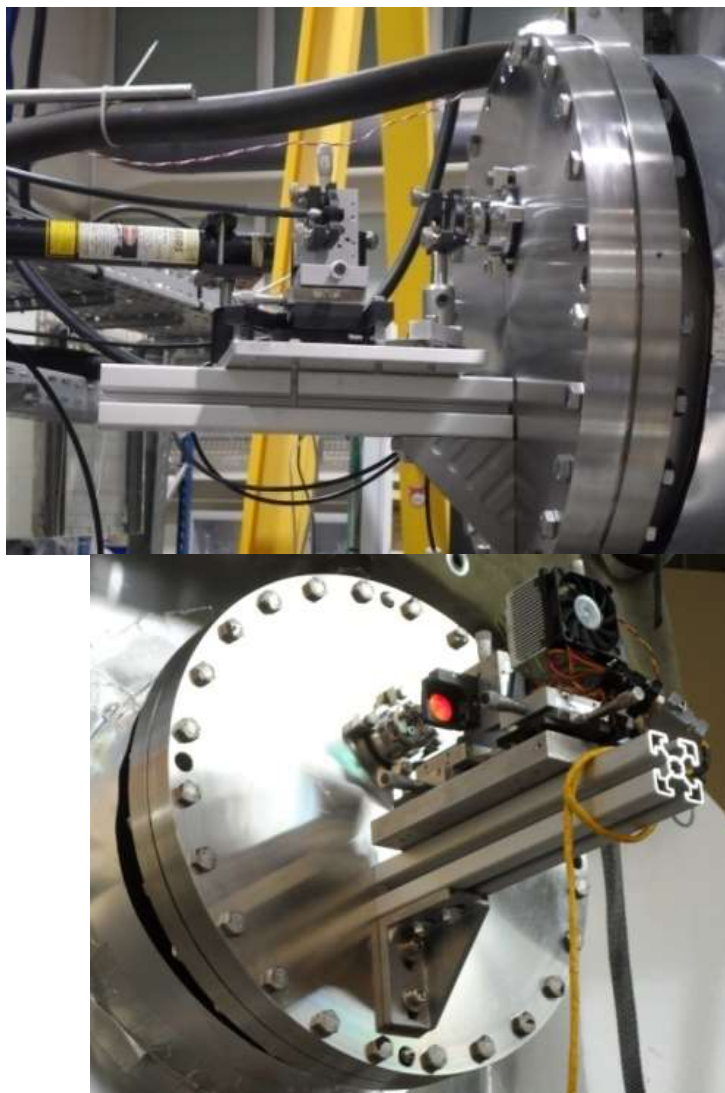
Species	IBI, base log10	Wavenumber (cm ⁻¹)	Spectrum origin / References
NO ₂	$(1.25 \pm 0.05) \times 10^{-18}$	2830-2950	HITRAN database
CH ₂ O	$(1.27 \pm 0.1) \times 10^{-18}$	2600-2844	Home-made calibration with (Gratien et al., 2007)
Trans-HONO	$(10 \pm 1) \times 10^{-18}$	1200-1300	Synthetic spectrum (Barney et al., 2001)
H ₂ O vapor	$(2.67) \times 10^{-17}$	1150-2150	HITRAN database and home-made spectra for high water concentration

540



545 Figure 1 Schematics of the experimental set-ups and devices installed around the CESAM chamber for intercomparison: IBBCEAS, NitroMAC, FT-IR spectrometer, NO_x analyzer, temperature and relative humidity sensor (T-RH sensor), pressure gauge.

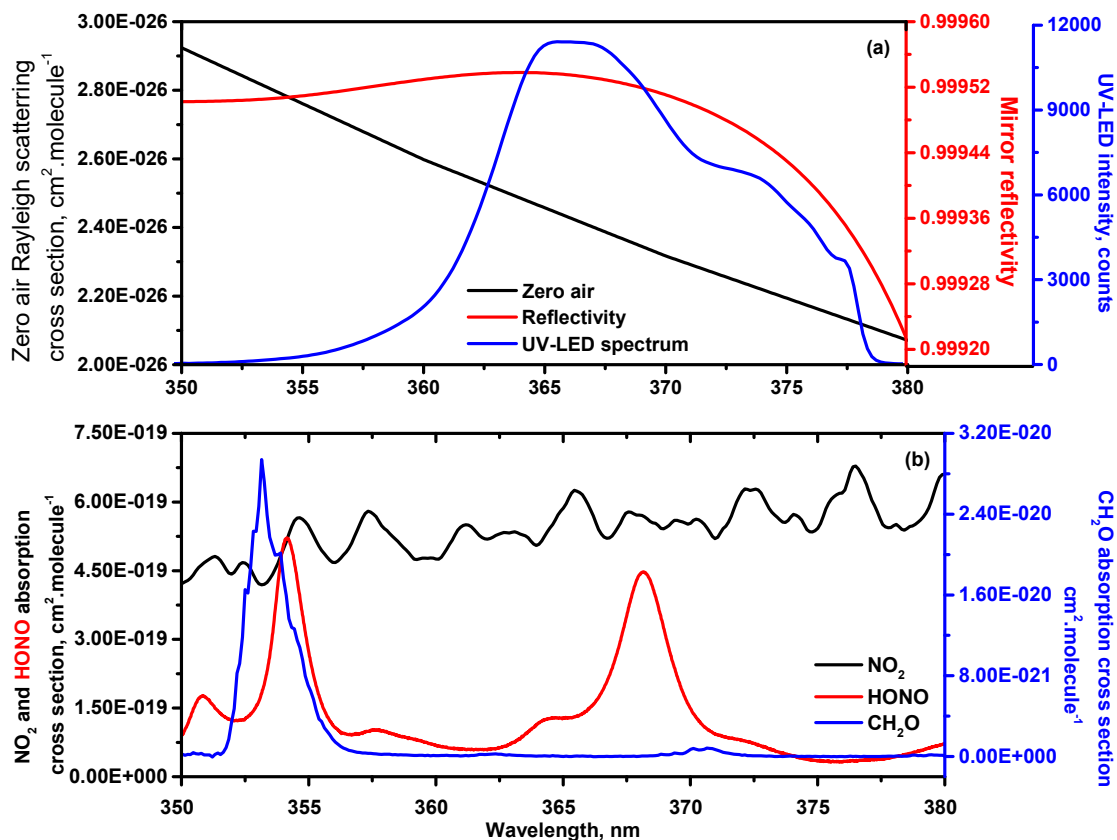




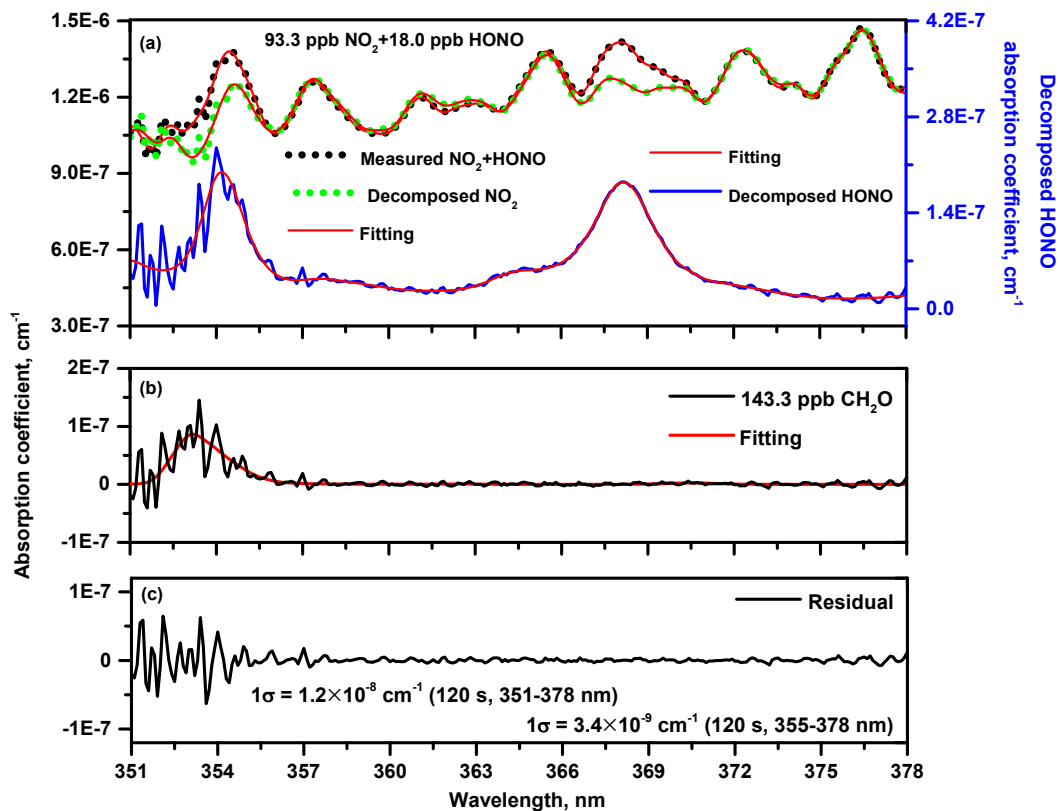
550

Figure 2 View of the IBCEAS installation on the CESAM simulation chamber flanges





555 Figure 3 Spectral region of 350-380 nm for IBBCEAS measurements: (a) UV-LED emission spectrum (blue), wavelength-dependent mirror reflectivity (red) and Rayleigh scattering cross section of zero air (black); (b) NO_2 (black), HONO (red) and CH_2O (blue) absorption cross sections.



560

Figure 4 Measured and fitted NO₂, HONO and CH₂O spectra associated with the related residual.



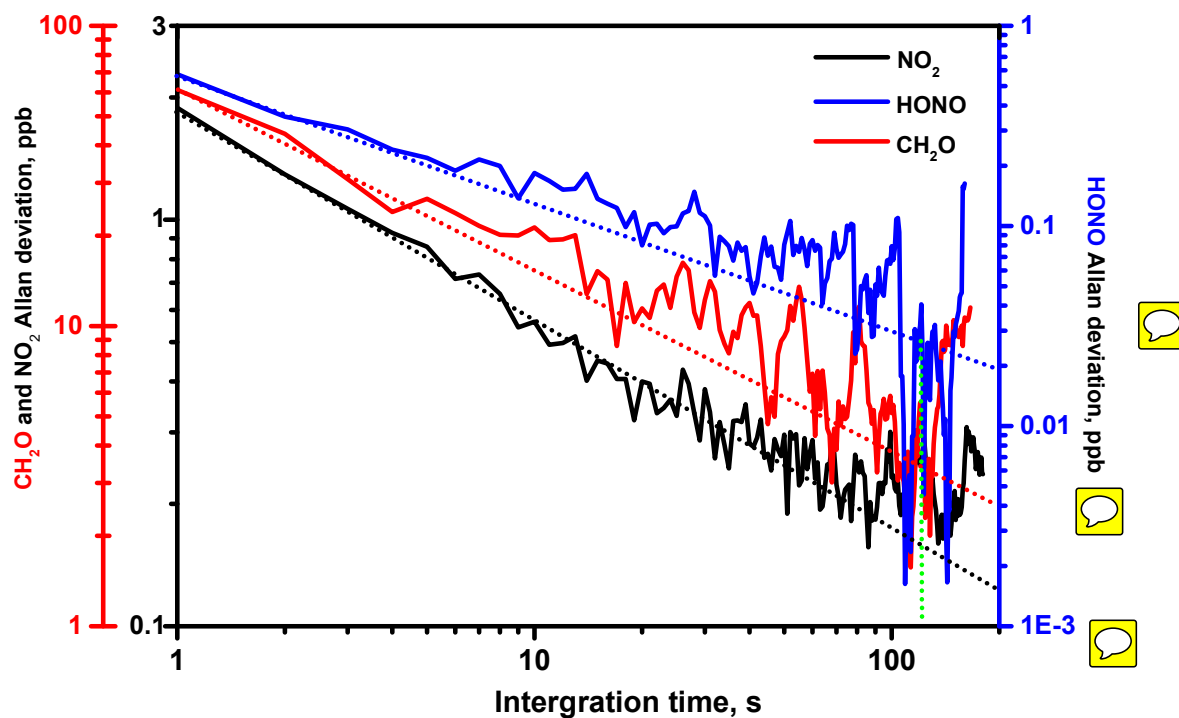
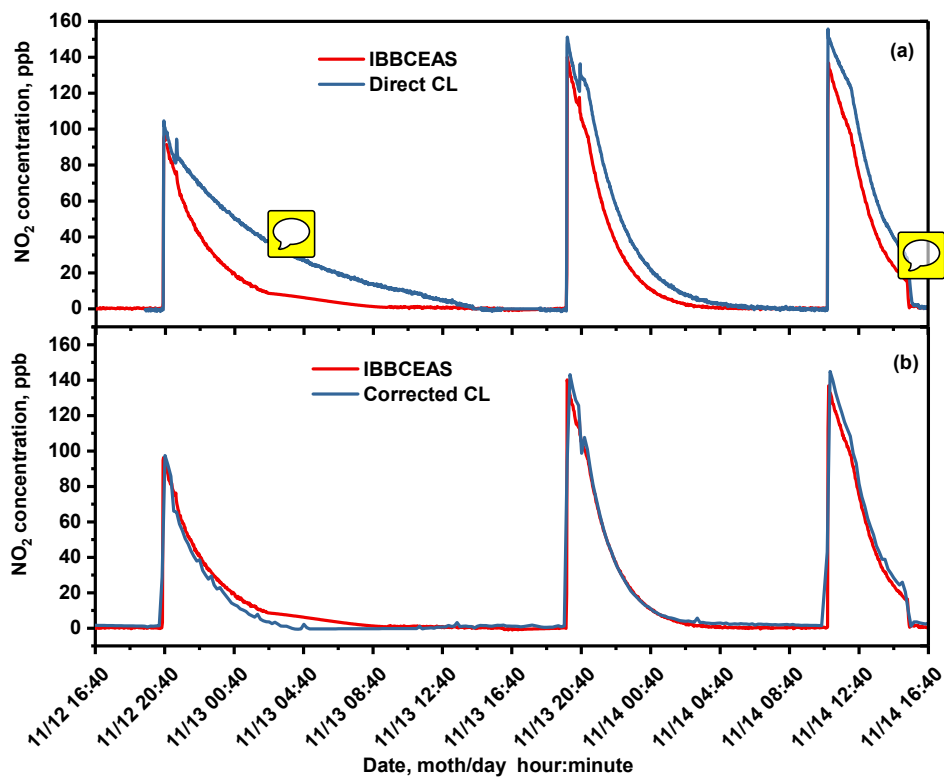
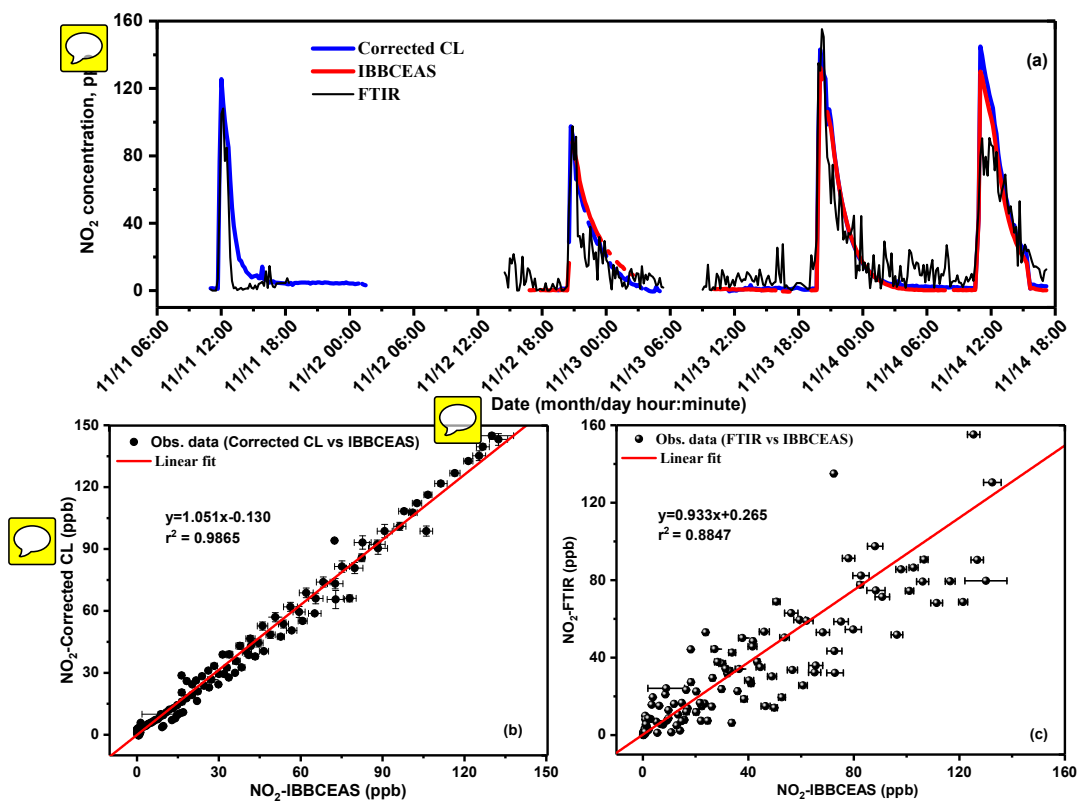


Figure 5 Allan deviation analysis for UV-LED IBBCEAS performance evaluation.



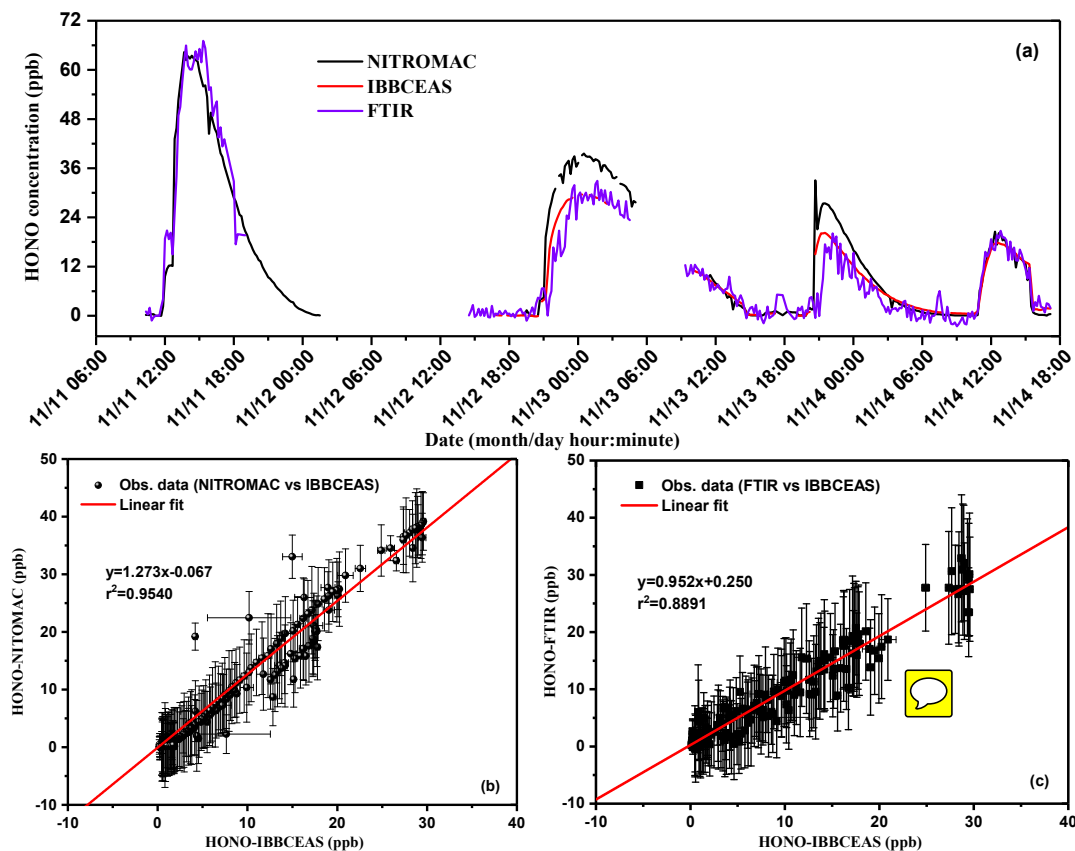
565

Figure 6 Investigation of positive interferences from nitrogen containing species (here: HONO) in NO_x analyzer (CL) measurement, in comparison with UV-LED-IBBCEAS measurement: (a) from CL-NO_x analyzer without HONO correction; (b) CL-NO_x analyzer results after HONO correction.



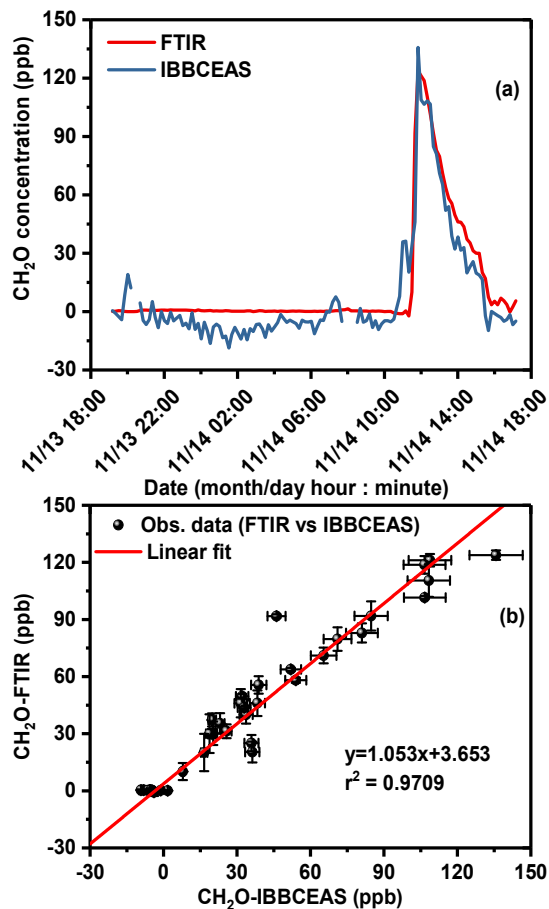
570

Figure 7 (a) Intercomparison measurement for NO₂ detection between IBBCEAS, FTIR and NO_x analyzer after HONO interference correction; (b) Correlation of the measured NO₂ concentrations between UV-LED-IBBCEAS and NO_x analyzer with HONO interferences correction; (c) Correlation of the measured NO₂ concentrations between UV-LED-IBBCEAS and FTIR.



575

Figure 8 (a): HONO intercomparison measurements between IBBCEAS, NitroMAC and FTIR; (b): Regressions analysis for the correlation of the measured HONO concentrations using UV-LED-IBBCEAS and NitroMAC; (c): Correlation of the measured HONO concentrations between UV-LED-IBBCEAS and FTIR.



580 Figure 9 Intercomparison measurements of CH₂O between IBBCEAS and FTIR: (a) Time series measurements of CH₂O concentrations from UV-LED IBBCEAS and FTIR; (b) Linear regression of the measured CH₂O in Fig. 9(a) : IBBCEAS (x-axis) versus FTIR (y-axis).